Tissue-specific dynamin-1 deletion at the calyx of Held decreases short-term depression through a mechanism distinct from vesicle resupply

Satyajit Mahapatra[a], Fan Fan[a], and Xuelin Lou[a,1]

[a]Department of Neuroscience, School of Medicine and Public Health, University of Wisconsin–Madison, Madison, WI 53706

Edited by Pietro De Camilli, Yale University and Howard Hughes Medical Institute, New Haven, CT, and approved April 19, 2016 (received for review October 22, 2015)

Dynamin is a large GTPase with a crucial role in synaptic vesicle regeneration. Acute dynamin inhibition impairs neurotransmitter release, in agreement with the protein's established role in vesicle resupply. Here, using tissue-specific dynamin-1 knockout [conditional knockout (cKO)] mice at a fast central synapse that releases neurotransmitter at high rates, we report that dynamin-1 deletion unexpectedly leads to enhanced steady-state neurotransmission and consequently less synaptic depression during brief periods of high-frequency stimulation. These changes are also accompanied by increased transmission failures. Interestingly, synaptic vesicle resupply and several other synaptic properties remain intact, including basal neurotransmission, presynaptic Ca^{2+} influx, initial release probability, and postsynaptic receptor saturation and desensitization. However, acute application of Latrunculin B, a reagent known to induce actin depolymerization and impair bulk and ultrafast endocytosis, has a stronger effect on steady-state depression in cKO than in control and brings the depression down to a control level. The slow phase of presynaptic capacitance decay following strong stimulation is impaired in cKO; the rapid capacitance changes immediately after strong depolarization are also different between control and cKO and sensitive to Latrunculin B. These data raise the possibility that, in addition to its established function in regenerating synaptic vesicles, the endocytosis protein dynamin-1 may have an impact on short-term synaptic depression. This role comes into play primarily during brief high-frequency stimulation.

short-term plasticity | release site clearance | dynamin | bulk endocytosis | actin

Sustained neurotransmission requires synaptic vesicle (SV) recycling. The reformation of functional SVs, in general, requires several seconds or even longer (1, 2) and is thus several orders of magnitude slower than vesicle release at active zones (AZs). Vesicle fusion can reach rates of up to a few thousand vesicles per second in many types of nerve terminals, such as ribbon synapses (3,000/s) (3), cerebellar basket cell terminals (5,000/s) (4), and the calyx of Held (6,000/s) (5–7). Because release sites are limited in number, synapses need to reuse them rapidly in succession during repetitive stimulation, and this requirement may be more restrictive than that of SV availability (8). AZs are composed of a meshwork of evolutionarily conserved scaffold proteins including RIM, Munc-13, RIM-BP, α-liprin, ELKS, and Ca^{2+} channels (9–11), but their dynamic properties are poorly understood (10). During high-frequency release, vesicle membrane components (12) and soluble N-Ethylmaleimide sensitive factor (NSF) attachment protein receptor (SNARE) proteins that occupy the release sites need to be cleared rapidly so that new vesicles can dock and prime for new rounds of exocytosis. The recovery of release sites may become rate-limiting during high rates of transmitter release (8). However, direct experimental testing is challenging due to the transient nature of this process. The molecular mechanism underlying site clearance and functional recovery are unclear. Tight exo/endocytosis coupling (13, 14) may contribute to the reavailability of release sites by promoting clearance of vesicle components from release sites during high synaptic activity (8). Refractoriness of release sites during high-frequency release had already been considered early on by Bernhard Katz (15). It was further supported by evidence for ultrastructural changes in AZs after stimulation (16, 17) and by studies on the temperature-sensitive dynamin mutant *shibire* in *Drosophila* (18) and on the perturbations of other proteins involved in endocytosis (19–21).

The calyx of Held is a fast central synapse in the auditory brainstem, and it spontaneously fires action potentials (APs) at ∼70 Hz [ranging between 0.4 and 174 Hz in postnatal day 32 (P32) mice] (22) or ∼30 Hz (median frequency in P13–28 mice) (23) in vivo. It can follow AP input at up to ∼500 Hz under sound stimulation in anesthetized mice (23, 24). The calyx of Held may reuse its release sites at least 3–5 times per second during transient high-frequency stimulation (8). This makes it an ideal model synapse for the study of rapid processes during endocytosis and release site clearance.

Dynamin is a large guanosine triphosphatase (GTPase) with multiple domains interacting with other molecules, and it is critical for membrane fission during vesicle trafficking (25). Among three dynamin isoforms (encoded by *Dnm1*, *Dnm2*, and *Dnm3*) in the mammalian brain, dynamin-1 is the most abundant (26). The conventional deletion of dynamin-1 causes early lethality in mice and accumulation of clathrin-coated endocytic intermediates at nerve terminals (26, 27). Direct presynaptic recordings from the calyx of Held in conventional dynamin-1 KO

Significance

Endocytosis is crucial for sustained synaptic transmission. During high-frequency neurotransmission, endocytosis recycles vesicular components rapidly and may promote the clearance of used SNAREs and other membrane proteins from release sites. We report that tissue-specific dynamin-1 deletion significantly reduces synaptic depression during bursts of the high-frequency stimulation at the mature calyx of Held in mice. This effect is contrary to the expected consequence of reduced recycling and cannot be explained by the commonly known mechanisms underlying short-term depression. Rather, the data imply that endocytosis may have a rapid, retrograde effect on transmitter release (e.g., through alterations of release site clearance) during high rates of synaptic vesicle fusion. Our finding indicates a role of dynamin-1 in high-frequency synaptic transmission and short-term plasticity.

Author contributions: S.M., F.F., and X.L. designed research; S.M., F.F., and X.L. performed research; S.M., F.F., and X.L. analyzed data; and S.M. and X.L. wrote the paper.

The authors declare no conflict of interest.

This article is a PNAS Direct Submission.

Freely available online through the PNAS open access option.

[1]To whom correspondence should be addressed. Email: xlou3@wisc.edu.

This article contains supporting information online at www.pnas.org/lookup/suppl/doi:10.1073/pnas.1520937113/-/DCSupplemental.

animals reveal a significant impairment of the slow form of endocytosis and a reduction of presynaptic Ca^{2+} currents (28). Further deletion of dynamin-3 exacerbates dynamin-1 KO phenotypes (29) and leads to striking synaptic facilitation (30). The spontaneous *Dnm1* mutation (R256L) in dogs causes an exercise-induced collapse syndrome (31), and *fitful* mice carrying a *Dnm1* mutation exhibit epilepsy (32). The *shibire* mutation paralyzes *Drosophila* at the restrictive temperature due to synaptic vesicle depletion at neuromuscular junctions (33). It also displays a rapid enhancement of synaptic depression within 20 ms of stimulation presumably arising from rapid obstruction of release sites (18).

Here, we examine how dynamin loss affects fast synaptic transmission at the mature calyx of Held (P16–20) by tissue-specific *Dnm1* gene deletion. To our surprise, the loss of dynamin-1 decreased short-term synaptic depression during brief high-frequency stimulation. This effect depends on the high-frequency stimulation and actin polymerization. Interestingly, the vesicle resupply rate, along with other properties of synaptic transmission, remains intact in conditional knockout (cKO) synapses. These data call for roles of dynamin in short-term synaptic plasticity in addition to its known function in regenerating new SVs. Mechanisms, which imply more efficient release site clearance in cKO than control during brief high-frequency stimulation, are discussed.

Results

Tissue-Specific Dynamin-1 Ablation Does Not Affect Basal Neurotransmission at the Mature Calyx of Held. Dynamin-1 was selectively ablated in mouse auditory brainstem by crossing $Dnm1^{f/f}$ (34) and $Krox20^{Cre}$ (35, 36). These conditional dynamin-1 knockout mice ($Dnm1^{\Delta/f}$ $Krox20^{Cre}$, hereafter named cKO) were viable, fertile, and without notable outward defects. This contrasts with the conventional dynamin-1 KO mice (26) and their out-breeding KO strain (crossing with CD-1) (28) that showed a much shorter life span (<2 wk) and smaller (~1/3 or less) body size and weight than that of the control. The morphology of the calyx of Held in cKO mice was indistinguishable from control (Fig. 1*B*, *Left*) with comparable, well-developed presynaptic structures at P20. Immunostaining showed abundant fluorescence of a synaptic marker vesicular glutamate transporter 1 (vGlut-1) in both control and cKO synapses, but dynamin-1 fluorescence nearly disappeared in cKO synapses (Fig. 1*B*, *Middle*), suggesting efficient dynamin-1 deletion in the cKO calyx of Held.

We first monitored the spontaneous miniature excitatory postsynaptic currents (mEPSCs) in the medial nucleus of trapezoid body (MNTB) neurons. The mEPSCs in cKO showed similar kinetics and amplitudes as those in control (control: −60.3 ± 3.7 pA, n = 15 synapses; cKO: −61.7 ± 3.8 pA, n = 17 synapses). The mEPSC frequency in cKO (cKO: 3.9 ± 0.7 Hz, n = 17) was slightly smaller than that of control (5.5 ± 0.6 Hz, n = 15; P = 0.076) (Fig. 1 *C–E*). The initial EPSCs induced by APs had comparable amplitudes (Fig. 1 *F–H*, control: −6.9 ± 0.4 nA, n = 35 synapses; cKO: −5.9 ± 0.5 nA, n = 50 synapses, P = 0.14) and half-widths (543 ± 26.8 μs, n = 35 for control; 541 ± 20.6 μs, n = 50 for cKO; P = 0.96) between the two groups. The EPSC latency in cKO was slightly longer than control (1.07 ± 0.02 ms for control; 1.15 ± 0.03 ms for cKO; P < 0.05). These findings demonstrate that basal transmission in a circuit of the central nervous system is nearly intact in the absence of dynamin-1, suggesting that dynamin-1 is not essential for low levels of synaptic activity. The remaining levels of vesicle recycling may be supported by dynamin-2 and -3 in the calyx of Held. These data are consistent with the nearly intact basal neurotransmission observed in conventional KO synapses (28). However, the conventional KO results in somewhat smaller presynaptic Ca^{2+} current and correspondingly smaller EPSCs; such changes were not observed in cKO mice.

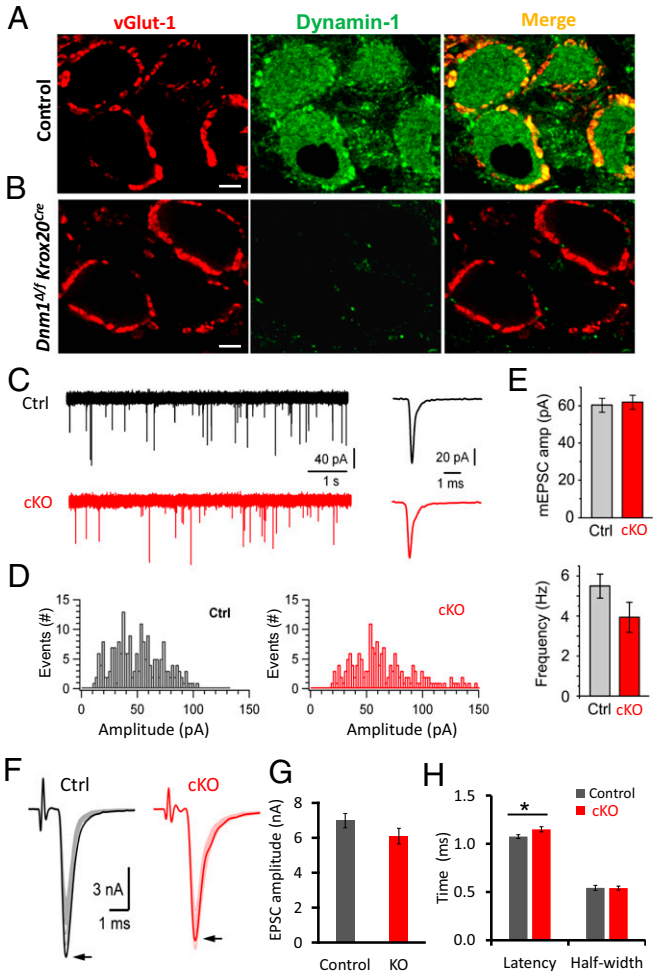

Fig. 1. Tissue-specific ablation of dynamin-1 has no major impact on the morphology of the calyx of Held and on basal synaptic transmission. (*A* and *B*) Immunofluorescence of the mature calyx of Held (P20) from a control and a cKO brain slice. Antibodies against the vesicular glutamate transporter-1 (red) and dynamin-1 (green, polyclonal antibody) were used. Note the disappearance of dynamin-1 fluorescence in cKO. (Scale bars: 5 μm.) (*C*, *Left*) Representative mEPSCs from MNTB neurons (P16–20). (*Right*) The averaged mEPSC traces from a control (222 events) and a cKO (n = 171 events) cell shown on the left. (*D*) mEPSC amplitude distribution from a control and a cKO synapse. (*E*) Amplitude and frequency of mEPSCs in both control (n = 15 synapses; total events: 4,414) and cKO groups (n = 17 synapses; total events: 3,614). (*F*) Representative control and cKO EPSCs evoked by 30 APs at 1 Hz. Arrows indicate the first EPSC peak. (*G* and *H*) EPSC amplitudes (*G*) and kinetics (*H*) from both control (n = 35) and cKO calyx of Held (n = 50) (P < 0.05 for the latency, Student's t test).

The Lack of Dynamin-1 Increases Steady-State Transmitter Release and Reduces Short-Term Depression During High-Frequency Stimulation. The calyx of Held can follow AP stimulation over a wide range of frequencies in vivo (23). We therefore examined the changes in EPSCs during AP stimulation at different frequencies in MNTB neurons. The steady-state depression levels were calculated based on the average value of the last five normalized EPSCs. We define depression as the complement to steady-state release that is expressed as a percentage of the first EPSC. In response to the low-frequency AP stimulation (30 APs at 10 Hz, Fig. 2 *A* and *B*), cKO synapses showed moderate depression (47.3 ± 5.0%, n = 10) similar to that in controls (54.2 ± 2.1%, n = 12; P = 0.23). However, in response to 300-Hz APs, cKO synapses showed much less depression than controls (Fig. 2 *C* and *D*), and steady-state

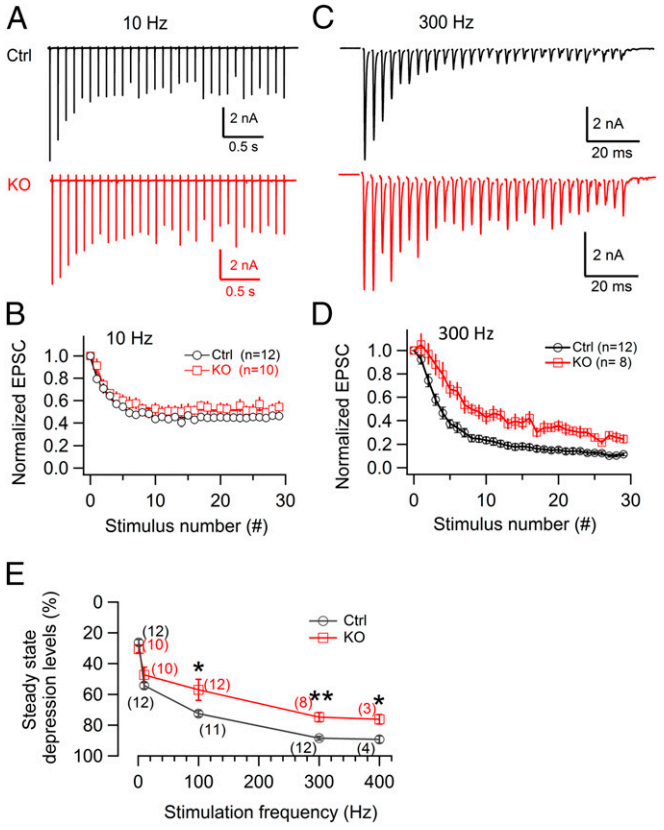

Fig. 2. Lack of dynamin-1 causes a relative increase in steady-state transmitter release and less synaptic depression during high-frequency stimulation. (*A*) Representative control and cKO EPSC trains in response to 30 APs at 10 Hz. (*B*) Average short-term depression (STD) curves at 10 Hz from control ($n = 12$) and cKO ($n = 10$) synapses ($\tau = 0.27$ s for both groups) showed no difference in STD. (*C*) As in *A* but in response to APs at 300 Hz. Note the larger EPSCs at the end of the train in cKO. (*D*) Average STD curves at 300 Hz in cKO ($\tau_{fast} = 7.9$ ms, $\tau_{slow} = 74$ ms; $n = 8$ synapses) and control ($\tau_{fast} = 12.2$ ms, $\tau_{slow} = 123$ ms; $n = 12$ synapses). The less depression in cKO compared with control was evident within a few stimuli (~10 ms) as their respective depression curves started separating. (*E*) The average STD levels in control and cKO synapses were plotted over different stimulation frequencies. Note that the difference in STD between control and cKO is frequency-dependent. The steady-state depression levels were calculated as the average value of the last five normalized EPSCs in each train from individual synapses; the number in each parentheses indicates the cell number recorded for that frequency. For any single data point in *E*, the numbers of animals that we used were from a minimum of three to four mice to a maximum of seven to eight mice.

release was larger in cKO. The average depression was significantly less in cKO (74.8 ± 3.03%, $n = 8$ synapses) than in control (88.5 ± 1.23%, $n = 12$ synapses; $P = 0.0016$) (Fig. 2*D*). This effect developed very rapidly during high-frequency stimulation so that depression curves diverged within a few AP stimuli (within ~10 ms) (Fig. 2*D*). Furthermore, this effect strongly depended on the stimulation frequency (Fig. 2*E*), as shown by the separation of the two traces at 100 Hz or higher.

The reduced synaptic depression in cKO observed here is consistent with the weaker depression that is observed at synapses lacking syndapin-1 (37), a critical dynamin-interacting partner. Along the same line, dynamin-1 and -3 double knockout synapses even exhibit strong facilitation, which is largely accounted for by a pronounced decrease in release probability and vesicle number (30). On the other hand, the reduction in depression in cKO synapses was unexpected because acute dynamin GTPase inactivation (18) or inhibition (20, 21) enhanced synaptic depression. An involvement of the *Krox20*^{Cre} gene in the depression phenotype of cKO synapses can be ruled out because the *Krox20*$^{Cre/+}$ gene alone did not change short-term synaptic depression (Fig. S1).

We also noted that synaptic transmission in cKO was more prone to fail than in control during high-frequency stimulation (Fig. S2). Further characterization of AP transmission revealed that the cKO calyx of Held could faithfully transmit APs at low frequencies (Fig. S3 *A* and *B*), but failed frequently at high frequencies (Fig. S3*C*). This was unexpected because the mature calyx of Held is known as a high-fidelity synapse (22, 38, 39). The transmission failures in cKO depended on both stimulation frequency (Fig. S2 *A* and *B*) and duration (Fig. S3 *E* and *F*). Interestingly, they occurred before synaptic vesicle depletion as indicated by the complete and sudden (rather than gradual) EPSC disappearance (Fig. S3 *E* and *F*, *Insets*). Further loose-patch recordings, in which local current signals from presynaptic and postsynaptic sites can be distinguished (Fig. S4*A*), revealed more frequent presynaptic AP failures than quantal failures in cKO synapses (Fig. S4 *B* and *C*).

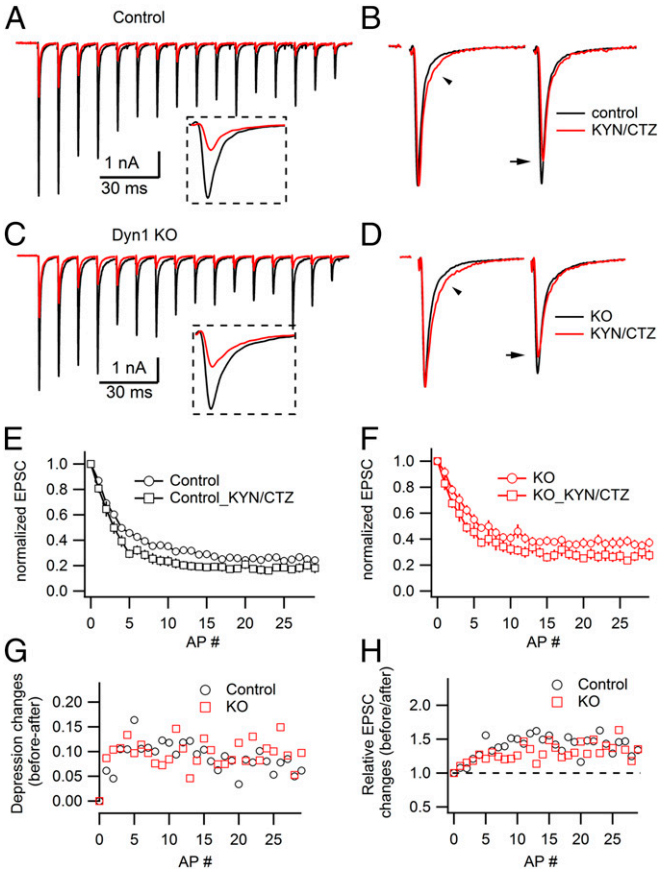

Fig. 3. Postsynaptic receptor saturation and desensitization do not contribute to the smaller STD at mature cKO calyx of Held. (*A*) EPSC changes before (black) and after (red) the application of 1 mM KYN and 100 μM CTZ during a train of 30 APs at 100 Hz in a control synapse. (*Inset*) Enlarged view of the first EPSCs under two conditions. (*B*) The first two normalized EPSCs showed substantial overlap before and after KYN/CTZ exposure. Note the slightly slower EPSC decay kinetics (arrowhead) and a minor decrease in the second EPSC peak (arrow) after applying KYN/CTZ (red). (*C* and *D*) Similar to *A* and *B*, but in a cKO synapse. (*E* and *F*) Average changes of STD with and without 1 mM KYN and 100 μM CTZ in control (*E*) ($n = 21$ and 9 synapses without and with KYN/CTZ, respectively) and cKO synapses (*F*) ($n = 35$ and 10 synapses without and with KYN/CTZ, respectively). Both groups showed a small but significant decrease of STD ($P < 0.05$). (*G* and *H*) Equal contribution of postsynaptic factors to 100 Hz STD in both control and cKO groups.

The Lack of Dynamin-1 Does Not Significantly Affect the Common Factors Underlying Synaptic Depression. To further explore the mechanism underlying the altered short-term depression in cKO synapses, we examined whether other factors known to influence short-term depression (STD) (40–43) account for the results. First, the changes in postsynaptic receptor saturation and desensitization are known to contribute to synaptic depression in the juvenile calyx of Held (44, 45). We used 1 mM kynurenic acid (KYN) and 100 μM cyclothiazide (CTZ) to reduce AMPA receptor saturation and desensitization, respectively. We found similar effects of these drugs in both control and cKO synapses. Normalized EPSCs before and after KYN + CTZ application nearly overlapped, with only slightly slower EPSC decay under KYN + CTZ (Fig. 3 *B* and *D*). These results speak against a major role of AMPA receptor saturation and desensitization in the mature calyx of Held in both control and cKO, in agreement with the previous study (45). Under this condition, synaptic depression was slightly enhanced to an equal extent in both control and cKO (Fig. 3 *E*–*H*).

Second, a decrease in presynaptic Ca^{2+} influx through voltage-gated Ca^{2+} channels might effectively decrease synaptic depression (46–48) because of the supralinear relationship between intracellular Ca^{2+} and transmitter release (7, 49). A recent study suggests the presence of homeostatic regulation of presynaptic Ca^{2+} influx at the neuromuscular junction (50). To explore this possibility, we performed direct presynaptic whole-cell recordings at the P13–15 calyx of Held. There was no difference in Ca^{2+} current amplitude and density between control and cKO synapses (Fig. 4 *A* and *B*). A relevant question is activity-dependent Ca^{2+} current facilitation because it modulates neurotransmission even with undistinguishable Ca^{2+} influx under basal conditions (51). We thus applied 30 AP-like (AP-L) pulses (1 ms, +30 mV, 333 Hz) to mimic afferent AP activity (Fig. 4*C*). Both control and cKO synapses showed significant Ca^{2+} current facilitation, but there was no difference in their amplitudes between control (1.07 ± 0.031) and cKO (1.1 ± 0.021 for the average of last 10 points; $P = 0.58$) (Fig. 4*D*). This excludes the potential involvement of the changes in presynaptic Ca^{2+} influx and activity-dependent facilitation in the STD phenotype in cKO synapses.

Third, a decrease in release probability (P_r) can cause less synaptic depression or even facilitation after the loss of dynamin-1, as we showed previously in dynamin-1, -3 double KO synapses (30), the terminals of which are largely vesicle-depleted and have accumulated abundant clathrin-coated profiles (29). We used two different approaches to assess a putative P_r change in the cKO calyx of Held. First, we examined the paired-pulse ratio (PPR) of EPSCs as a P_r indicator. We observed no significant difference in PPRs between control and cKO over a wide range of frequencies up to 200 Hz (Fig. S5). At 300 Hz or above, PPRs in cKO changed from depression to facilitation, indicating a selective enhancement of transmitter release under the high-frequency stimulation. It is noteworthy that the PPR is an indirect indicator of P_r that may have certain limitations (52). We therefore estimated P_r using an alternative approach by calculating the ratio of the first EPSC amplitude divided by its own readily releasable pool (RRP) in each synapse. The RRP size was measured using 100 Hz train stimulation in the presence of KYN + CTZ (Fig. S6) (44). We found no significant difference in P_r between control and cKO synapses, despite the fact that the RRP size was slightly smaller in cKO than in control (Fig. S6). Given the limitations of this method of estimating RRP (53), this method may underestimate RRP size, particularly in cKO which has the enhanced steady-state release. To accurately measure RRP, we turned to direct presynaptic capacitance measurements with strong depolarization (50 ms, 0 mV). This experiment demonstrated comparable RRP sizes between control and cKO (Fig. 7 *A* and *B*). These results, plus equal sizes of AP evoked EPSCs between two groups, suggest a similar P_r in cKO compared with control. Thus, an alteration in initial P_r appears unlikely to be the major factor that accounts for the reduced depression in cKO synapses, but the contribution of minor P_r decrease cannot be ruled out at very high frequencies (≥300 Hz).

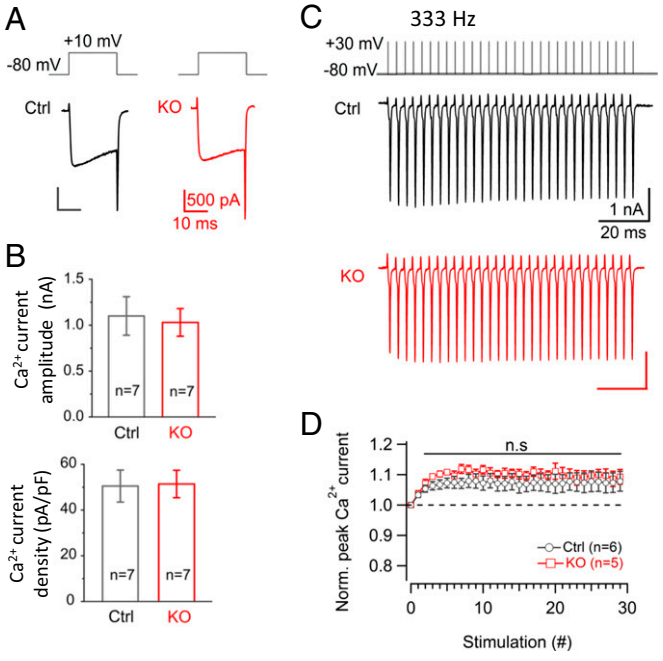

Fig. 4. Presynaptic Ca^{2+} influx and Ca^{2+} current facilitation in cKO synapses are comparable to control. (*A*) Representative presynaptic Ca^{2+} currents evoked by a single depolarizing pulse (+10 mV, 20 ms) at a calyx of Held from control and cKO mice (P13–15). (*B*) Ca^{2+} current amplitude and density between control and cKO synapses ($n = 7$ in each group). (*C*) The 333-Hz, AP-like 30 pulses (top, +30 mV, 1 ms) triggered a small but significant facilitation of presynaptic Ca^{2+} current both in control and in cKO synapses. (*D*) A comparable amplitude of Ca^{2+} current facilitation in control ($n = 6$) and in cKO ($n = 5$, $P = 0.62$ and 0.58 for the last 5- and 10-point averages, respectively) synapses.

Vesicle Resupply Is Intact After Brief High-Frequency APs in the Absence of Dynamin-1. The balance between vesicle pool depletion and rapid vesicle replenishment during high-frequency stimulation is crucial for short-term plasticity. Genetic perturbation of endocytic proteins often leads to a delay in vesicle resupply, as shown in mutants of endophilin (54–56), synaptojanin (57, 58), and dap160/intersectin-1 (59). Intersectin-1 KO synapses in mice showed deficient vesicle replenishment even without a detectable change in capacitance decays (60). We tested the vesicle resupply rate by examining the recovery of transmission evoked by an AP at different intervals following each high-frequency stimulation (30 APs at 300 Hz) (Fig. 5*A*). Transmission recovery was measured as the ratio of the test EPSC amplitude relative to the first EPSC in each train. Consistent with the two phases of Ca^{2+}-dependent recovery (61), transmission recovered with a double-exponential time course, with no significant difference between control (τ_{fast} = 0.13 s, 30%; τ_{slow} = 3.3 s, 57%) and cKO synapses (τ_{fast} = 0.15 s, 14%; τ_{slow} = 3.5 s, 63%) (Fig. 5*B*). This indicates a normal rate of vesicle resupply following brief high-frequency stimulation in cKO, which is not surprising given the presence of a large pool of recycling vesicles in this type of synapses (40, 62, 63). It is noteworthy that the recovery curve in cKO started with a significantly higher initial level (0.26 ± 0.017, $n = 5$) than in control (0.15 ± 0.016, $n = 12$, $P < 0.01$) (Fig. 5*A*). This is consistent with less depression at steady state in cKO synapses (Fig. 2*C*).

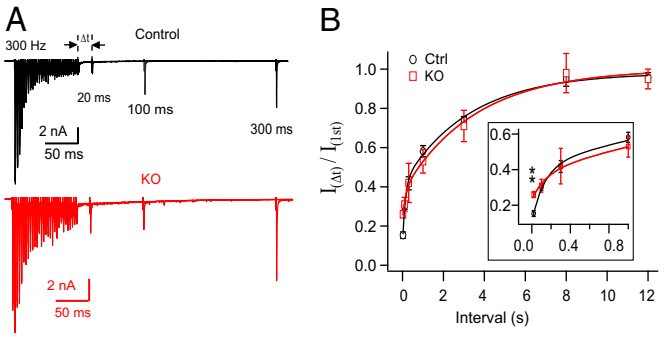

Fig. 5. Synaptic transmission recovery from the short-term depression is intact in the absence of dynamin-1. (*A*) Synaptic transmission at different time intervals (Δt = 0.02, 0.1, 0.3, 1, 3, 8, 12 s) after the 300-Hz AP train. Synapses were allowed to rest for at least 20 s between trials. (*B*) The time course of the transmission recovery curves from STD in control (τ_{fast} = 0.13 s, 30%; τ_{slow} = 3.3 s, 57%; n = 12) and in cKO (τ_{fast} = 0.15 s, 14%; τ_{slow} = 3.5 s, 63%; n = 5) synapses were similar. Only synapses without failure were analyzed for both control and cKO groups. (*Inset*) The recovery curves at expanded time scales to show the significantly higher starting level of recovery in cKO synapses.

As an alternative estimate of vesicle resupply, we measured the RRP recovery rate with a pair of 100-Hz trains at different time intervals (Δt) in the presence of 1 mM KYN and 100 μM CTZ (Fig. S7*A*). We found that RRP recovery was unchanged in cKO synapses (τ = 1.5 s) compared with control (τ = 1.3 s) (Fig. S7*B*). These data are consistent with intact vesicle resupply (Fig. 5) and also agree with the intact RRP recovery after dynamin inhibition by pipette infusion of 0.3 mM GTPγS (64). Therefore, a lack of dynamin-1 does not affect the vesicle resupply to AZs following brief high-frequency stimulation at the mature calyx of Held.

Actin Depolymerization Has a Stronger Effect on Synaptic Depression in cKO than in Control Synapses. It is known that dynamin regulates actin function through direct and indirect interactions (65) and that the loss of dynamin strongly enhances actin reorganization (34, 66). Therefore, actin may differentially contribute to endocytosis, as well as transmitter release, in cKO and control synapses. Indeed, previous studies of ultrastructure reported an increase in bulk endocytosis—a fast and efficient membrane retrieval mechanism primarily induced during very intense stimulation—in synapses lacking dynamin-1 (67). In addition, it was shown that actin plays an important role in bulk and ultrafast endocytosis (68–72). These observations raise the possibility that an actin-dependent increase in bulk endocytosis in cKO could make release site clearance more efficient than in control during high-frequency release. If this is the case, inhibition of actin polymerization and bulk endocytosis is expected to slow down endocytosis and release site clearance and thereby accelerate the depression.

To test this idea, we acutely inhibited actin polymerization using Latrunculin-B (Lat-B, 15 μM) (73) in brain slices. Lat-B caused a significant decrease of steady-state release after a 200-Hz AP train (Fig. 6 *A* and *B*) in control, without significantly changing the initial EPSC amplitude (−9.3 ± 1.4 nA with Lat-B, −8.45 ± 1.2 nA without Lat-B; n = 7 each; P = 0.64). This is consistent with a previous study (73). However, Lat-B in cKO produced a much greater effect on synaptic depression at 200 Hz and brought synaptic depression to the same level as in control (7.2 ± 0.5%, n = 7 for control; 7.8 ± 0.8%, n = 5 for cKO; P = 0.46) (Fig. 6 *B* and *D*). Lat-B abolished the difference in the depression levels between control and cKO at both low and high frequencies (Fig. 6*E*). These data, together with normal transmission recovery, are consistent with the possibility that we mentioned above.

The Properties of Presynaptic Endocytosis in the Calyx of Held from Dynamin-1 cKO Mice. We performed direct presynaptic membrane capacitance (Cm) recordings and observed a large Cm increase at P8–10 calyx of Held. After a 50-ms depolarization (0 mV, with 0.2 mM Cs–EGTA in the pipette solution), the amplitudes of the Cm increases and presynaptic Ca^{2+} currents were comparable between control and cKO synapses (P = 0.58 and 0.21, respectively) (Fig. 7 *A*–*C*), suggesting similar sizes of RRPs between the two groups. Next, we monitored the dynamics of endocytosis after different stimulation protocols and characterized the Cm levels of a fast phase (at 2 s) and a slow phase (at 35 s) (with 0.5 mM Cs–EGTA in the pipette solution). We first applied mild stimulation using 30 AP-L pulses at 333 Hz to mimic high-frequency AP activity. Both control and cKO synapses showed moderate exocytosis followed by similar levels of Cm recovery at 2 s and at

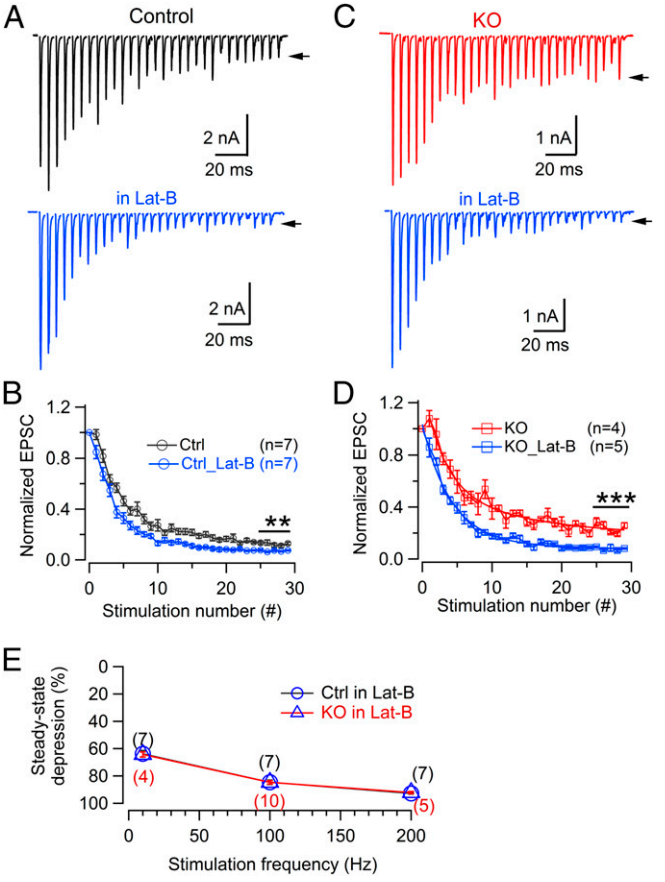

Fig. 6. Disruption of actin polymerization eliminates the difference in STD between control and cKO synapses during high-frequency stimulation. (*A* and *B*) Latrunculin-B (15 μM) marginally enhanced steady-state depression in control synapses at 200 Hz (30 APs) without significantly changing EPSC amplitude. Two recordings shown in *A* were from different terminals in control mice; arrows indicate the peak of the last EPSC. Note the small STD difference (0.13 ± 0.01, no Lat-B, n = 7 synapses; 0.072 ± 0.005, with lat-B, n = 7 synapses; P = 0.006). (*C* and *D*) The Lat-B effect in cKO synapses. Note that steady-state depression under the normal condition in cKO (0.24 ± 0.02, n = 4 synapses) comes down strongly in the presence of Lat-B (0.078 ± 0.008, n = 5 synapses; P < 0.001), reaching a level that is comparable to controls. (*E*) Steady-state depression levels in the presence of Lat-B (calculated as the average of the last 5 points in each train of individual recording) at different stimulation frequencies. The number in each parentheses indicates the synapse number recorded at that frequency; three to seven mice were used for each data point.

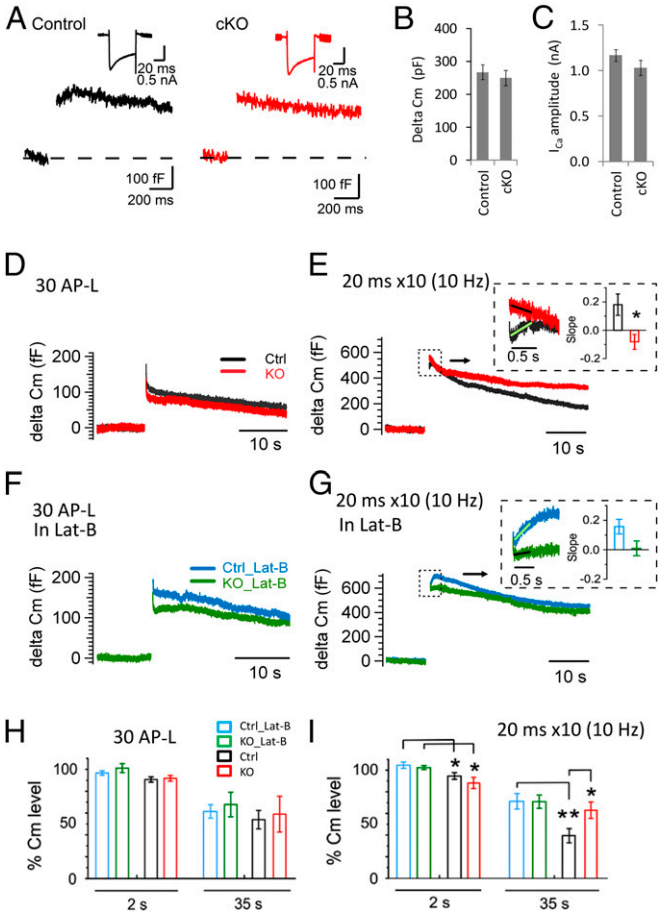

Fig. 7. Exocytosis and endocytosis examined by capacitance measurements at the calyx of Held under the normal condition and in the presence of Latrunculin-B. (*A*) A typical Cm trace induced by a 50-ms depolarization (0 mV) at P8–10 calyx of Held. (*B* and *C*) Average delta Cm (control: 270 ± 22 fF, $n = 12$; cKO: 250 ± 23 fF, $n = 16$; $P = 0.58$) and presynaptic Ca^{2+} currents in control (1.17 ± 0.06 nA, $n = 12$) and cKO synapses (1.03 ± 0.08 nA, $n = 16$; $P = 0.21$). (*D*) Average presynaptic Cm changes at the calyx of Held (P8–10) under mild stimulation (30 AP-like pulses at 333 Hz, +30 mV for 1 ms). (*E*) Cm changes under strong stimulation (10 × 20 ms, 0 mV, 100-ms interval). (*Inset*) An expanded view of the average Cm traces within 1 s after stimulation (control slope: 0.18 ± 0.07 fF, $n = 7$; cKO slope: −0.08 ± 0.05, $n = 5$; $P = 0.017$). (*F*) Average Cm changes after the mild stimulation in the presence of Lat-B (15 μM). (*G*) Average Cm changes after strong stimulation in the presence of Lat-B (15 μM). (*Inset*) The expanded view of Cm changes and slopes in control and in cKO (control: 0.16 ± 0.05, $n = 6$; cKO: 0.0053 ± 0.05, $n = 7$; $P = 0.052$). (*H*) Summary of Cm decays after mild stimulation (30 AP-L at 333 Hz) under the normal condition and in Lat-B for control and cKO. The data showed the relative Cm levels remaining at 2 s (control: 90.5 ± 2.4%, $n = 7$; cKO: 91.5 ± 2.6%, $n = 8$; $P = 0.8$) and at 35 s from the end of stimulation (control: 53.9 ± 8.4%, $n = 6$; cKO: 58.8 ± 11.5%, $n = 6$; $P = 0.75$). In the presence of Lat-B, the Cm levels at 2 s (control: 97.0 ± 2.0%, $n = 7$; cKO: 101.2 ± 4.1%, $n = 8$; $P = 0.35$) and at 35 s (control: 61.5 ± 6.1%, $n = 7$; cKO: 67.8 ± 11.2%; $P = 0.64$). (*I*) As in *H* but after strong stimulation (20-ms depolarization × 10 at 10 Hz). The Cm levels after strong stimulation at 2 s (control: 94.4 ± 3.1%, $n = 7$; cKO: 88.0 ± 5.2%, $n = 5$; $P = 0.33$) and at 35 s (control: 39.4 ± 6.7%, $n = 7$; KO: 62.9 ± 7.6%, $n = 5$; $P = 0.04$). In the presence of Lat-B, the Cm levels at 2 s (control: 105 ± 2.9%, $n = 6$; cKO: 102.3 ± 1.8%, $n = 7$; $P = 0.53$) and at 35 s (control: 71.2 ± 7.3%, $n = 6$; cKO: 70.9 ± 6.2%, $n = 7$; $P = 0.98$). Student's *t* test was used for statistical comparison between the two groups in *H* and *I*.

35 s (Fig. 7 *D* and *H*). After strong stimulation with depolarizing pulses (10 × 20 ms, 0 mV, at 10 Hz); however, we observed a large Cm increase (524 ± 54 fF, $n = 7$ for control; 555 ± 62 fF, $n = 5$ for KO; $P = 0.84$) (Fig. 7*E*). Again, the decay was biphasic with the second phase significantly slower in cKO than in controls (Cm level at 35 s in control: 39.4 ± 6.7%, $n = 7$; KO: 62.9 ± 7.6%, $n = 5$; $P = 0.04$) (Fig. 7 *E* and *I*). The fast phase of Cm decay (at 2 s) in cKO tended to be faster (decreased to 88.0 ± 5.2% of its peak, $n = 5$) than in control (to 94.4 ± 3.1%, $n = 7$; $P = 0.33$). These data agree well with our previous work showing a pronounced impairment in the second Cm decay phase after strong but not after mild stimulation (28), as well as impaired clathrin-coated endocytosis under the electron microscope in dynamin-1 KO terminals (26, 28, 67). Remaining dynamin-2 and -3 may be sufficient to support low levels of endocytosis and transmission in the absence of dynamin-1.

It was reported that bulk endocytosis as observed by electron microscopy is coupled in time to strong stimulation (67, 74). We reasoned that Cm changes immediately after strong stimulation may capture, at least a part of, bulk endocytosis. We therefore focused on Cm changes within half a second after depolarization. It is known that Cm changes in this time window can be affected significantly by many factors, such as gating currents (75, 76), high levels of asynchronous release after strong stimulation, and/or other processes irrelevant to transmitter release (77, 78). Therefore, they are often disregarded in Cm studies of endocytosis, including in our previous work (28). On the other hand, direct comparison of these signals between control and cKO under the same experimental conditions may still provide useful information on the fast endocytosis because these factors are expected to be equally present in both groups. We found that initial Cm decreases right after weak stimulation (30 AP-L at 333 Hz) were similar between control and cKO (Fig. 7*D*), confirming equal contributions of these various factors under the same stimulation condition. Cm transients immediately after strong stimulation (10-Hz, 20-ms train), however, were clearly different in cKO, compared with control (Fig. 7*E*, *Inset*). Most cKO synapses (four of five cells) showed a net decrease in initial Cm (cKO slope: −0.08 ± 0.05, $n = 5$) during half a second after the train (Fig. 7*E*, *Inset*), contrasting with transient Cm increases (control slope: 0.18 ± 0.07 fF, $n = 7$; $P = 0.017$) observed in the majority of control synapses (five of seven).

Next, we examined the role of actin depolymerization induced by Lat-B (15 μM) on Cm changes. With mild stimulation (30 AP-L at 333 Hz), Lat-B slightly increased the exocytosis and showed a trend of slowing down the Cm decay at 2 s in both control and cKO, although differences were not statistically significant (Fig. 7 *F* and *H* and Fig. S8 *A*, *C*, and *E*). With the strong stimulation (10 × 20 ms at 10 Hz), however, Lat-B nearly abolished the fast Cm decay (Fig. 7*G*, *Inset* and Fig. S8 *B*, *D*, and *F*) and significantly reduced the membrane retrieval during the first 2 s in both control ($P = 0.035$) and cKO synapses ($P = 0.048$) (Fig. 7*I*) (compared with the normal conditions without Lat-B; Fig. 7*E*, *Inset* and Fig. S8 *B* and *F*). The slow phase (at 35 s) was significantly slower in control ($P = 0.0084$), but not in cKO synapses ($P = 0.43$, compared with those without Lat-B) (Fig. S8 *B*, *D*, and *F*). We closely examined initial Cm changes within half a second after stimulation and compared the responses between conditions with and without Lat-B (Fig. 7 *E* and *G*, *Insets*). We found that Lat-B abolished the fast Cm decrease and led to a nearly flat or even increasing Cm trace in cKO. There was only a minor difference in Cm changes in control between conditions with and without Lat-B application. Cm slopes between control (0.16 ± 0.05, $n = 6$) and cKO (0.0053 ± 0.05, $n = 7$; $P = 0.052$) in the presence of Lat-B were comparable. Despite the technical limitations, these data indicate that actin-dependent fast endocytosis (e.g., bulk endocytosis) may become important under strong stimulation to balance the rapid exocytosis load and that Lat-B has different effects on Cm decays between cKO and control.

Discussion

We examined synaptic transmission at the mature calyx of Held using tissue-specific dynamin-1 KO and found an unexpected

reduction in synaptic depression during brief high-frequency AP stimulation. This reduction in synaptic depression in cKO depends on neither vesicle availability to AZs nor other common factors underlying synaptic depression, but it does rely on actin polymerization. Actin depolymerization differentially affects the short-term depression in control and cKO, as well as endocytosis. Our finding indicates an important role of dynamin-1 in repetitive transmitter release and short-term synaptic depression in native brain circuitry, in addition to its established role in regenerating and supplying new synaptic vesicles for long-term neurotransmission.

We have systematically characterized synaptic transmission in the cKO calyx of Held, including mEPSC amplitude and frequency, evoked EPSCs, action potential waveform, presynaptic Ca^{2+} influx and facilitation, postsynaptic receptor saturation and desensitization, RRP size, and vesicle resupply rate. These factors are largely intact in cKO synapses and unlikely to account for the reduction of synaptic depression observed in cKO.

One simple explanation for this phenotype is a P_r decrease in the cKO calyx of Held. A larger PPR at frequencies above 300 Hz appears to support this idea (Fig. S5). However, PPRs were not statistically different over a wide range of frequencies (<300 Hz) despite their tendency to be slightly higher. Other assessments of release probability (using the ratio of single AP-evoked EPSC divided by the RRP) pointed toward a similar initial P_r in the two groups. These observations suggest that a P_r change in cKO synapses, if it exists, should be very small. Therefore, a P_r decrease in cKO appears unlikely to be the major factor to account for the depression phenotype in cKO. Nevertheless, a contribution of a P_r change cannot be ruled out at very high frequencies (e.g., >300 Hz).

Another possible explanation for the decreased depression in cKO is an enhanced release site clearance at AZs. This process might rapidly become rate-limiting during high rates of transmitter release (8, 15). Rapid local membrane remodeling and protein sorting/diffusion may facilitate site clearance at the subsecond timescale through fast membrane retrieval (long before slow endocytosis comes into play). Multiple forms of fast endocytosis that have high efficiency in retrieving membrane, such as bulk endocytosis and ultrafast endocytosis, have been documented (2, 14, 28, 67, 74, 79, 80). It has also been reported that bulk endocytosis as observed by electron microscopy increases significantly (approximately twofold) during intense stimulation in the absence of dynamin-1 (27, 67). It is likely that an up-regulated actin-dependent mechanism (e.g., bulk endocytosis) in cKO promotes release site clearance during high-frequency stimulation, leading to enhanced transmitter release and reduced depression. If so, the availability of release sites might rapidly emerge as a rate-limiting step during brief high-frequency release in the calyx of Held. Future work using novel techniques, such as fast superresolution imaging (21, 81) or pulse-chase flash-freezing electron microscopy (14), is required to investigate the local membrane dynamics, protein sorting, and diffusion at the millisecond timescale. Nanometer resolution imaging of AZs under high rates of transmitter release conditions needs to be achieved. New approaches that can selectively regulate fast endocytosis are also needed to address this fundamental question.

The greater effect of Lat-B on synaptic depression in cKO compared with control (Fig. 6) correlates well with its larger effect on the inhibition of the Cm decrease immediately after a depolarization in cKO (Fig. 7 *E* and *G*, *Insets*), indicating that both processes may be related through an actin-dependent mechanism. Dynamin can regulate actin function through direct and indirect interactions (65, 82), and actin is important for bulk (68–70) and ultrafast endocytosis (72). Interestingly, dynamin KO leads to alteration of actin polymerization and reorganization in other types of cells (34, 66). A role for actin in vesicle recruitment has also been reported (73, 83, 84). Similarly, Lat-B caused an apparent enhancement in short-term depression in our study. This effect can be explained by inadequate vesicle recruitment to AZs and/or insufficient clearance of SV components (e.g., SNARE proteins) from AZs; the latter may prevent the rapid reavailability of the limited release sites for new rounds of vesicle docking and priming during high rates of release. We favor the latter interpretation under our experimental conditions because the vesicle resupply rate in cKO is comparable to that in the control (Fig. 5 and Fig. S7).

The role of dynamin in short-term synaptic depression has been assessed in previous work with different results, using the *shibire* mutant in *Drosophila* (18) or dynasore (20, 21). It is unclear how these differences come out. A common property in previous dynamin inhibition studies is that GTPase-inactivated dynamin is not physically removed from synapses. Dominant-negative effects of these inactivated dynamin molecules and/or some off-target effects of inhibitors (85) may explain, at least in part, the discrepancy. For example, the inactivated dynamin contains multiple interacting domains that may sequester their interaction partners (such as endophilin and syndapin) in clathrin-coated pits (CCPs) and result in a different endocytic defect. This effect is highlighted by a study showing that the accumulated CCPs on the plasma membrane (PM) in *shibire* mutants are converted into large bulk *cisternae* following the further photo-inactivation of dynamin (all of the domains) (86). The dynamin inhibitors or else inactivation can have off-target effects. For example, dynasore affects actin polymerization (in dynamin-1, -2, and -3 triple KO cells) (85), intracellular Ca^{2+} levels, mEPSC frequency (87), and bulk endocytosis possibly through actin perturbation or syndapin sequestration (68, 85).

Developmental compensation appears unlikely to account for the results of cKO because compensation should weaken or mask the phenotype (i.e., no changes in depression), but we observed the opposite (i.e., significantly less depression). In addition, the cKO mice were outwardly normal, and their nerve terminals showed no compensatory dynamin-3 increases (Fig. S9). The puncta redistribution of dynamin-3 observed in neuronal cultures (26) was not evident in the cKO calyx of Held.

Discrepancies between dynamin KO and dynamin inhibition have been consistently reported in other studies. For example, synaptic ultra-structures are very different after stimulation between *shibire* mutants (nearly empty terminals with abundant CCPs on the PM) (88) and dynamin KO (abundant large vacuoles and some CCPs) (27, 29, 67). Likewise, a spontaneous dynamin-1 point mutation in *fitful* mice causes enhanced depression (32) with a phenotype similar to *shibire*, albeit less severe, highlighting the discrepancy between dynamin-1 inhibition and deletion (KO) in the same species. Remarkably, despite these discrepancies, our findings and previous studies (18, 20, 21) point to a potential regulatory effect of the same process during exocytosis and endocytosis coupling, implying that alterations in release site clearance may be an overlooked mechanism for modulation of short-term plasticity during high-frequency transmitter release.

Materials and Methods

Generation of Conditional Dynamin-1 KO Selectively in Mouse Auditory Brainstem. The tissue-specific dynamin-1 conditional KO mice were generated by crossing the $Dnm1^{f/f}$ mice (34) and the $Krox20^{Cre}$ mice (36). The KO mice were viable and fertile with similar body weight and size, which contrasts with the short life span (<2 wk) and much smaller body size (1/3 of the control size or less at P12) of the conventional dynamin-1 KO mice after outbreeding with the CD1 strain (28). Littermates carrying no $Krox20^{Cre}$ were used as controls unless otherwise specified. All animal care and use were approved by Animal Care and Use Committees at the University of Wisconsin–Madison. See *SI Materials and Methods* for details.

Immunofluorescence Staining and Confocal Imaging. Mouse brains (P18–20) were fixed and cut into 40- to 60-μm slices. Immunohistochemistry and confocal fluorescence imaging were performed as described previously (66). See *SI Materials and Methods* for details.

Brain Slices, Patch Clamp, and Presynaptic Capacitance Measurements. Brain slices (180–200 μm) containing MNTBs were prepared from P16–20 mice unless otherwise specified, and patch clamp recordings were made as previously described (44). The extracellular solution (ES, in mM): 120 NaCl, 2.5 KCl, 25 $NaHCO_3$, 1.25 NaH_2PO_4, 2 $CaCl_2$, 1 $MgCl_2$, 25 glucose, 3 myoinositol, 2 Na-Pyruvate, 0.4 (L-)ascorbic acid (pH 7.4 with 95% O_2 and 5% CO_2 bubbling). Strychnine–HCl (2 μM), 10 μM bicuculline, and 50 μM D-AP_5 were routinely included in extracellular solution for EPSC recordings. EPSCs were evoked by a bipolar electrode, and no offline R_s correction was applied. Cm was measured using the Sine+DC technique under whole-cell patch clamp as described previously (28, 66). Cm levels (%) after endocytosis recovery in fast and slow phases were calculated at 2 and 35 s, respectively. For details of EPSC recordings and Cm measurements, see *SI Materials and Methods*. All experiments were conducted at room temperature (20–22 °C).

Data Analysis and Statistics. Electrophysiology data were analyzed with IgorPro (WaveMetrics). Values were presented as mean ± SEM, statistical analyses were performed using two-tail Student's *t* test, and significance level was set at $P < 0.05$, denoted with asterisks (*$P < 0.05$, **$P < 0.01$, ***$P < 0.001$). See *SI Materials and Methods* for details.

ACKNOWLEDGMENTS. We thank Patrick Charnay and Ralf Schneggenburger for providing *Krox20*^{Cre} mice; Pietro DeCamilli and Shaw Ferguson for *Dnm1*$^{f/f}$ mice and for very helpful discussions; Charles Wollitz, Jaffna Mathiaparanam, Elizabeth Westrick, and Juliana Maedke for technical support; and Meyer Jackson, Ed Chapman, Tim Gomez, and Erwin Neher for reading the manuscript and helpful suggestions. This work is supported by National Institutes of Health Grants R01DK093953 (to X.L.) and P30NS069271 and Brain Research Foundation Grant BRFSG201407 (to X.L.).

1. Saheki Y, De Camilli P (2012) Synaptic vesicle endocytosis. *Cold Spring Harb Perspect Biol* 4(9):a005645.
2. Wu LG, Ryan TA, Lagnado L (2007) Modes of vesicle retrieval at ribbon synapses, calyx-type synapses, and small central synapses. *J Neurosci* 27(44):11793–11802.
3. Heidelberger R, Heinemann C, Neher E, Matthews G (1994) Calcium dependence of the rate of exocytosis in a synaptic terminal. *Nature* 371(6497):513–515.
4. Sakaba T (2008) Two Ca(2+)-dependent steps controlling synaptic vesicle fusion and replenishment at the cerebellar basket cell terminal. *Neuron* 57(3):406–419.
5. Schneggenburger R, Neher E (2000) Intracellular calcium dependence of transmitter release rates at a fast central synapse. *Nature* 406(6798):889–893.
6. Bollmann JH, Sakmann B, Borst JG (2000) Calcium sensitivity of glutamate release in a calyx-type terminal. *Science* 289(5481):953–957.
7. Lou X, Scheuss V, Schneggenburger R (2005) Allosteric modulation of the presynaptic Ca2+ sensor for vesicle fusion. *Nature* 435(7041):497–501.
8. Neher E (2010) What is rate-limiting during sustained synaptic activity: Vesicle supply or the availability of release sites. *Front Synaptic Neurosci* 2:144.
9. Gundelfinger ED, Fejtova A (2012) Molecular organization and plasticity of the cytomatrix at the active zone. *Curr Opin Neurobiol* 22(3):423–430.
10. Sigrist SJ, Schmitz D (2011) Structural and functional plasticity of the cytoplasmic active zone. *Curr Opin Neurobiol* 21(1):144–150.
11. Südhof TC (2012) The presynaptic active zone. *Neuron* 75(1):11–25.
12. Takamori S, et al. (2006) Molecular anatomy of a trafficking organelle. *Cell* 127(4): 831–846.
13. Haucke V, Neher E, Sigrist SJ (2011) Protein scaffolds in the coupling of synaptic exocytosis and endocytosis. *Nat Rev Neurosci* 12(3):127–138.
14. Watanabe S, et al. (2013) Ultrafast endocytosis at mouse hippocampal synapses. *Nature* 504(7479):242–247.
15. Katz B (1996) Neural transmitter release: From quantal secretion to exocytosis and beyond. The Fenn Lecture. *J Neurocytol* 25(12):677–686.
16. Heuser JE, et al. (1979) Synaptic vesicle exocytosis captured by quick freezing and correlated with quantal transmitter release. *J Cell Biol* 81(2):275–300.
17. Heuser JE, Reese TS (1981) Structural changes after transmitter release at the frog neuromuscular junction. *J Cell Biol* 88(3):564–580.
18. Kawasaki F, Hazen M, Ordway RW (2000) Fast synaptic fatigue in shibire mutants reveals a rapid requirement for dynamin in synaptic vesicle membrane trafficking. *Nat Neurosci* 3(9):859–860.
19. Kawasaki F, et al. (2011) The DISABLED protein functions in CLATHRIN-mediated synaptic vesicle endocytosis and exoendocytic coupling at the active zone. *Proc Natl Acad Sci USA* 108(25):E222–E229.
20. Hosoi N, Holt M, Sakaba T (2009) Calcium dependence of exo- and endocytotic coupling at a glutamatergic synapse. *Neuron* 63(2):216–229.
21. Hua Y, et al. (2013) Blocking endocytosis enhances short-term synaptic depression under conditions of normal availability of vesicles. *Neuron* 80(2):343–349.
22. Lorteije JA, Rusu SI, Kushmerick C, Borst JG (2009) Reliability and precision of the mouse calyx of Held synapse. *J Neurosci* 29(44):13770–13784.
23. Sonntag M, Englitz B, Kopp-Scheinpflug C, Rübsamen R (2009) Early postnatal development of spontaneous and acoustically evoked discharge activity of principal cells of the medial nucleus of the trapezoid body: An in vivo study in mice. *J Neurosci* 29(30):9510–9520.
24. Kopp-Scheinpflug C, Tolnai S, Malmierca MS, Rübsamen R (2008) The medial nucleus of the trapezoid body: Comparative physiology. *Neuroscience* 154(1):160–170.
25. Ferguson SM, De Camilli P (2012) Dynamin, a membrane-remodelling GTPase. *Nat Rev Mol Cell Biol* 13(2):75–88.
26. Ferguson SM, et al. (2007) A selective activity-dependent requirement for dynamin 1 in synaptic vesicle endocytosis. *Science* 316(5824):570–574.
27. Hayashi M, et al. (2008) Cell- and stimulus-dependent heterogeneity of synaptic vesicle endocytic recycling mechanisms revealed by studies of dynamin 1-null neurons. *Proc Natl Acad Sci USA* 105(6):2175–2180.
28. Lou X, Paradise S, Ferguson SM, De Camilli P (2008) Selective saturation of slow endocytosis at a giant glutamatergic central synapse lacking dynamin 1. *Proc Natl Acad Sci USA* 105(45):17555–17560.
29. Raimondi A, et al. (2011) Overlapping role of dynamin isoforms in synaptic vesicle endocytosis. *Neuron* 70(6):1100–1114.
30. Lou X, et al. (2012) Reduced release probability prevents vesicle depletion and transmission failure at dynamin mutant synapses. *Proc Natl Acad Sci USA* 109(8): E515–E523.
31. Patterson EE, et al. (2008) A canine DNM1 mutation is highly associated with the syndrome of exercise-induced collapse. *Nat Genet* 40(10):1235–1239.
32. Boumil RM, et al. (2010) A missense mutation in a highly conserved alternate exon of dynamin-1 causes epilepsy in fitful mice. *PLoS Genet* 6(8):e1001046.
33. Koenig JH, Saito K, Ikeda K (1983) Reversible control of synaptic transmission in a single gene mutant of Drosophila melanogaster. *J Cell Biol* 96(6):1517–1522.
34. Ferguson SM, et al. (2009) Coordinated actions of actin and BAR proteins upstream of dynamin at endocytic clathrin-coated pits. *Dev Cell* 17(6):811–822.
35. Han Y, Kaeser PS, Südhof TC, Schneggenburger R (2011) RIM determines Ca^2+ channel density and vesicle docking at the presynaptic active zone. *Neuron* 69(2):304–316.
36. Voiculescu O, Charnay P, Schneider-Maunoury S (2000) Expression pattern of a Krox-20/Cre knock-in allele in the developing hindbrain, bones, and peripheral nervous system. *Genesis* 26(2):123–126.
37. Koch D, et al. (2011) Proper synaptic vesicle formation and neuronal network activity critically rely on syndapin I. *EMBO J* 30(24):4955–4969.
38. Taschenberger H, von Gersdorff H (2000) Fine-tuning an auditory synapse for speed and fidelity: Developmental changes in presynaptic waveform, EPSC kinetics, and synaptic plasticity. *J Neurosci* 20(24):9162–9173.
39. McLaughlin M, van der Heijden M, Joris PX (2008) How secure is in vivo synaptic transmission at the calyx of Held? *J Neurosci* 28(41):10206–10219.
40. Schneggenburger R, Sakaba T, Neher E (2002) Vesicle pools and short-term synaptic depression: Lessons from a large synapse. *Trends Neurosci* 25(4):206–212.
41. Zucker RS, Regehr WG (2002) Short-term synaptic plasticity. *Annu Rev Physiol* 64: 355–405.
42. Fioravante D, Regehr WG (2011) Short-term forms of presynaptic plasticity. *Curr Opin Neurobiol* 21(2):269–274.
43. Dutta Roy R, Stefan MI, Rosenmund C (2014) Biophysical properties of presynaptic short-term plasticity in hippocampal neurons: Insights from electrophysiology, imaging and mechanistic models. *Front Cell Neurosci* 8:141.
44. Lou X, Korogod N, Brose N, Schneggenburger R (2008) Phorbol esters modulate spontaneous and Ca2+-evoked transmitter release via acting on both Munc13 and protein kinase C. *J Neurosci* 28(33):8257–8267.
45. Taschenberger H, Leão RM, Rowland KC, Spirou GA, von Gersdorff H (2002) Optimizing synaptic architecture and efficiency for high-frequency transmission. *Neuron* 36(6):1127–1143.
46. Catterall WA, Few AP (2008) Calcium channel regulation and presynaptic plasticity. *Neuron* 59(6):882–901.
47. Xu J, Wu LG (2005) The decrease in the presynaptic calcium current is a major cause of short-term depression at a calyx-type synapse. *Neuron* 46(4):633–645.
48. Nakamura T, Yamashita T, Saitoh N, Takahashi T (2008) Developmental changes in calcium/calmodulin-dependent inactivation of calcium currents at the rat calyx of Held. *J Physiol* 586(9):2253–2261.
49. Neher E, Sakaba T (2008) Multiple roles of calcium ions in the regulation of neurotransmitter release. *Neuron* 59(6):861–872.
50. Müller M, Davis GW (2012) Transsynaptic control of presynaptic Ca^{2+} influx achieves homeostatic potentiation of neurotransmitter release. *Curr Biol* 22(12):1102–1108.
51. Nanou E, Sullivan JM, Scheuer T, Catterall WA (2016) Calcium sensor regulation of the CaV2.1 Ca2+ channel contributes to short-term synaptic plasticity in hippocampal neurons. *Proc Natl Acad Sci USA* 113(4):1062–1067.
52. Branco T, Staras K (2009) The probability of neurotransmitter release: Variability and feedback control at single synapses. *Nat Rev Neurosci* 10(5):373–383.
53. Neher E (2015) Merits and limitations of vesicle pool models in view of heterogeneous populations of synaptic vesicles. *Neuron* 87(6):1131–1142.
54. Milosevic I, et al. (2011) Recruitment of endophilin to clathrin-coated pit necks is required for efficient vesicle uncoating after fission. *Neuron* 72(4):587–601.
55. Dickman DK, Horne JA, Meinertzhagen IA, Schwarz TL (2005) A slowed classical pathway rather than kiss-and-run mediates endocytosis at synapses lacking synaptojanin and endophilin. *Cell* 123(3):521–533.
56. Schuske KR, et al. (2003) Endophilin is required for synaptic vesicle endocytosis by localizing synaptojanin. *Neuron* 40(4):749–762.
57. Verstreken P, et al. (2003) Synaptojanin is recruited by endophilin to promote synaptic vesicle uncoating. *Neuron* 40(4):733–748.
58. Di Paolo G, et al. (2004) Impaired PtdIns(4,5)P2 synthesis in nerve terminals produces defects in synaptic vesicle trafficking. *Nature* 431(7007):415–422.
59. Koh TW, Verstreken P, Bellen HJ (2004) Dap160/intersectin acts as a stabilizing scaffold required for synaptic development and vesicle endocytosis. *Neuron* 43(2): 193–205.

60. Sakaba T, et al. (2013) Fast neurotransmitter release regulated by the endocytic scaffold intersectin. *Proc Natl Acad Sci USA* 110(20):8266–8271.
61. Wang LY, Kaczmarek LK (1998) High-frequency firing helps replenish the readily releasable pool of synaptic vesicles. *Nature* 394(6691):384–388.
62. de Lange RP, de Roos AD, Borst JG (2003) Two modes of vesicle recycling in the rat calyx of Held. *J Neurosci* 23(31):10164–10173.
63. Qiu X, Zhu Q, Sun J (2015) Quantitative analysis of vesicle recycling at the calyx of Held synapse. *Proc Natl Acad Sci USA* 112(15):4779–4784.
64. Wu XS, Wu LG (2009) Rapid endocytosis does not recycle vesicles within the readily releasable pool. *J Neurosci* 29(35):11038–11042.
65. Orth JD, McNiven MA (2003) Dynamin at the actin-membrane interface. *Curr Opin Cell Biol* 15(1):31–39.
66. Fan F, et al. (2015) Dynamin 2 regulates biphasic insulin secretion and plasma glucose homeostasis. *J Clin Invest* 125(11):4026–4041.
67. Wu Y, et al. (2014) A dynamin 1-, dynamin 3- and clathrin-independent pathway of synaptic vesicle recycling mediated by bulk endocytosis. *eLife* 3:e01621.
68. Nguyen TH, et al. (2012) Actin- and dynamin-dependent maturation of bulk endocytosis restores neurotransmission following synaptic depletion. *PLoS One* 7(5):e36913.
69. Shupliakov O, et al. (2002) Impaired recycling of synaptic vesicles after acute perturbation of the presynaptic actin cytoskeleton. *Proc Natl Acad Sci USA* 99(22): 14476–14481.
70. Holt M, Cooke A, Wu MM, Lagnado L (2003) Bulk membrane retrieval in the synaptic terminal of retinal bipolar cells. *J Neurosci* 23(4):1329–1339.
71. Gormal RS, Nguyen TH, Martin S, Papadopulos A, Meunier FA (2015) An acto-myosin II constricting ring initiates the fission of activity-dependent bulk endosomes in neurosecretory cells. *J Neurosci* 35(4):1380–1389.
72. Watanabe S, et al. (2014) Clathrin regenerates synaptic vesicles from endosomes. *Nature* 515(7526):228–233.
73. Lee JS, Ho WK, Lee SH (2012) Actin-dependent rapid recruitment of reluctant synaptic vesicles into a fast-releasing vesicle pool. *Proc Natl Acad Sci USA* 109(13):E765–E774.
74. Clayton EL, Evans GJ, Cousin MA (2008) Bulk synaptic vesicle endocytosis is rapidly triggered during strong stimulation. *J Neurosci* 28(26):6627–6632.
75. Kilic G, Lindau M (2001) Voltage-dependent membrane capacitance in rat pituitary nerve terminals due to gating currents. *Biophys J* 80(3):1220–1229.
76. Horrigan FT, Bookman RJ (1994) Releasable pools and the kinetics of exocytosis in adrenal chromaffin cells. *Neuron* 13(5):1119–1129.
77. Yamashita T, Hige T, Takahashi T (2005) Vesicle endocytosis requires dynamin-dependent GTP hydrolysis at a fast CNS synapse. *Science* 307(5706):124–127.
78. Wu W, Xu J, Wu XS, Wu LG (2005) Activity-dependent acceleration of endocytosis at a central synapse. *J Neurosci* 25(50):11676–11683.
79. Renden R, von Gersdorff H (2007) Synaptic vesicle endocytosis at a CNS nerve terminal: Faster kinetics at physiological temperatures and increased endocytotic capacity during maturation. *J Neurophysiol* 98(6):3349–3359.
80. Alabi AA, Tsien RW (2013) Perspectives on kiss-and-run: Role in exocytosis, endocytosis, and neurotransmission. *Annu Rev Physiol* 75:393–422.
81. Huang F, et al. (2013) Video-rate nanoscopy using sCMOS camera-specific single-molecule localization algorithms. *Nat Methods* 10(7):653–658.
82. Menon M, Schafer DA (2013) Dynamin: Expanding its scope to the cytoskeleton. *Int Rev Cell Mol Biol* 302:187–219.
83. Lee JS, Ho WK, Neher E, Lee SH (2013) Superpriming of synaptic vesicles after their recruitment to the readily releasable pool. *Proc Natl Acad Sci USA* 110(37):15079–15084.
84. Sakaba T, Neher E (2003) Involvement of actin polymerization in vesicle recruitment at the calyx of Held synapse. *J Neurosci* 23(3):837–846.
85. Park RJ, et al. (2013) Dynamin triple knockout cells reveal off target effects of commonly used dynamin inhibitors. *J Cell Sci* 126(Pt 22):5305–5312.
86. Kasprowicz J, Kuenen S, Swerts J, Miskiewicz K, Verstreken P (2014) Dynamin photoinactivation blocks Clathrin and α-adaptin recruitment and induces bulk membrane retrieval. *J Cell Biol* 204(7):1141–1156.
87. Douthitt HL, Luo F, McCann SD, Meriney SD (2011) Dynasore, an inhibitor of dynamin, increases the probability of transmitter release. *Neuroscience* 172:187–195.
88. Koenig JH, Ikeda K (1989) Disappearance and reformation of synaptic vesicle membrane upon transmitter release observed under reversible blockage of membrane retrieval. *J Neurosci* 9(11):3844–3860.